Biochemistry and Biophysics Reports 24 (2020) 100815

Contents lists available at ScienceDirect

Biochemistry and Biophysics Reports

journal homepage: www.elsevier.com/locate/bbrep

Probing the Structure–Function relationship and amyloidogenic propensities in natural variants of apolipoprotein A-I

Farah Ma'arfi [a], Subhash Chandra [b], Jamal e Fatima [a], Mohd Yasir Khan [c], Snober S. Mir [a], Mohd Aslam Yusuf [a,*]

[a] Department of Bioengineering, Integral University, Kursi Road, Dasauli, Lucknow, 226026, India
[b] School of Life Sciences, Jawaharlal Nehru University, New Delhi, 110067, India
[c] Department of Biosciences, Integral University, Kursi Road, Dasauli, Lucknow, 226026, India

ARTICLE INFO

Keywords:
Apolipoprotein A-I
Mutation
Amyloid
Atherosclerosis

ABSTRACT

Background: Apolipoprotein A-I (apoA-I) protects against atherosclerosis and participates in the removal of excess cellular cholesterol from peripheral organs. Several naturally occurring apoA-I mutations are associated with familial systemic amyloidosis, with deposition of amyloid aggregates in peripheral organs, resulting in multiple organ failure. Systematic studies on naturally occurring variants are needed to delineate their roles and involvement in pathogenesis.

Methods: We performed a comparative structure–function analysis of five naturally occurring apoA-I variants and the wild-type protein. Circular dichroism, Fourier-transform infrared spectroscopy, thioflavin T and congo red fluorescence assays, thermal, chemical, and proteolytic stability assays, and 1,2-Dimyristoyl-*sn*-glycero-3-phosphocholine clearance analyses were used to assess the effects of mutations on the structure, function, stability, aggregation, and proteolytic susceptibility of the proteins to explore the mechanisms underlying amyloidosis and hypercholesterolemia.

Results: We observed structural changes in the mutants independent of fibril formation, suggesting the influence of the surrounding environment. The mutants were involved in aggregate formation to varying degree; L170P, R173P, and V156E showed an increased propensity to aggregate under different physiological conditions. β sheet formation indicates that L170P and R173P participate in amyloid formation. Compared to WT, V156E and L170P exhibited higher capacity for lipid clearance.

Conclusions: The selected point mutations, including those outside the hot spot regions of apoA-I structure, perturb the physiochemical and conformational behavior of the protein, influencing its function.

General significance: The study provides insights into the structure–function relationships of naturally occurring apoA-I variants outside the hot spot mutation sites.

1. Introduction

Cardiovascular disease (CVD) is the topmost cause of human deaths worldwide, with atherosclerosis being the underlying cause of pathogenesis in most of the cases. Apolipoprotein A-I (apoA-I) is known to have a protective role against atherosclerosis [1]. It is synthesized in the liver and intestine as a pre-pro-protein. The mature protein has 243 amino acids and a molecular mass of 28 kDa [2]. ApoA1 exists in both free and lipid-bound forms [2]. It is a major protein of high-density lipoproteins (HDL) and is crucial in defining its size and shape. About 95% of apoA-I circulating in the plasma has stable α-helices bound to HDL, whereas, only 5% is present as labile lipid-free apoA-I monomer [3]. ApoA1 plays an important role in lipid metabolism as it solubilizes the lipid components of HDL, removes cholesterol from peripheral cells, and has a role in the activation of lecithin:cholesterol acyltransferase (LCAT) as well as in delivering cholesterol esters to the liver [4,5]. Owing to its role in reverse cholesterol transport (RCT), deficiency of apoA-I is directly associated with CVDs [6].

Several mutations are found in apoA-I that are responsible for HDL deficiency and increase the risk for CVDs [7]. However, some natural variants, such as R173C (apoA-I Milano), are known to protect against CVDs [8]. Many other apoA-I mutations are associated with

* Corresponding author. ;
E-mail address: aslamadhami@gmail.com (M.A. Yusuf).

https://doi.org/10.1016/j.bbrep.2020.100815
Received 14 June 2020; Received in revised form 9 September 2020; Accepted 13 September 2020

gain-of-toxic-function and are responsible for familial systemic amyloidosis caused by deposition of amyloid aggregates in organs, such as the heart, liver, kidney, nerves, ovary, and testis [9]. Most of the apoA-I mutations that give rise to amyloidosis result in the aggregation of the N-terminal fragment containing 1–93 amino acids. This region has a strong propensity for fibrillation and is found in amyloid plaques. Unmodified, full-length, wild type (WT) apoA-I does not show a tendency toward amyloidogenesis under most of the conditions known to promote amyloid formation. The amyloidogenic mutations are mostly found in two "hot-spot" regions (amino acid residues 1–100 and 173–178) of apoA-I. About 50% of the substitution mutations reside in the region from amino acid 50–93, and are associated with hepatic or renal amyloidosis [9,10]. On the other hand, several mutations in the amino acid region 173–178 specifically trigger amyloidosis in the heart, skin, and larynx. Irrespective of the location of mutations, limited proteolysis between residues 83–93 is mostly involved in all apoA-I amyloidoses. Thus, the N-terminal region of apoA-I is the most prominent region involved in the deposition of amyloid fibrils [11].

Perturbation in the overall structure of apoA-I is not necessary for it to become amyloidogenic; even a slight exposure of the major amyloid "hot spot" region increases the proteolytic susceptibility and induces a cooperative shift toward a misfolded conformation [12]. In the present study, we investigated the molecular basis of apoA-I amyloidosis and atherosclerosis by determining the effects of selected point mutations of apoA-I, including those outside the hot-spot regions, on its structure, function, and amyloidogenicity using various biophysical and biochemical methods. The mutants that were selected for this study included the natural variants of apoA-I reported in the literature, which are either responsible for impairing RCT or are amyloidogenic. Among the mutants selected, V156E and P143R are apoA-I loss-of function mutations that are implicated in alterations in LCAT and cholesterol efflux, gain-of-function mutations, L170P and R173P, which are known amyloidogenic mutants, and R173C, which is protective against atherosclerosis. The carriers of R173C exhibit enhanced RCT, anti-inflammatory, and plaque stabilizing activities [13]. These mutants reside in the central domain comprised of amino acids 144–186, which is known to participate in LCAT activation, lipid binding, and in the stability and maturation of HDL molecules [14,15].

2. Materials and methods

2.1. Materials

Escherichia coli strains used in this study were maintained and stored using the routine culture techniques. The pMD18-T vector containing the full-length apoA-I cDNA was purchased from Sino Biological Inc. (China). The pET28a (+) vector was from Novagen (Madison, WI). The culture media components were purchased from HiMedia (Mumbai, India). The enzymes and chemicals used for DNA manipulation were obtained from Thermo Scientific (USA). The 6 × His-purifying resin was from Novagen. The oligonuleotide primers, guanidine hydrochloride (GndHCl), thioflavinT (ThT), 4,4′-dianilino-1,1′-binaphthyl-5,5′-disulfonic acid dipotassium salt (bis-ANS), congo red, sodium dodecyl sulphate (SDS), agarose, anti-His tag (catalog no. H1029) and HRP-conjugated anti-mouse IgG were procured from Sigma-Aldrich (St Louis, MO). 1,2-dimyristoyl sn-*glycero*-3-phosphatidylcholine (DMPC) was from Avanti Polar Lipids (Alabaster, AL). The QuickChange II XL Site-Directed Muatgenesis kit was from Stratagene (LaJolla, CA). Coomassie Brilliant Blue R250 (CBB-R250) was obtained from Merck. Other reagents were of the highest analytical grade available, unless otherwise stated.

2.2. Cloning, expression, and purification of recombinant proteins

The apoA-I WT cDNA was cloned into the multiple cloning site of the linearized pET28a expression vector. The clone was verified by automated sequencing (GATC Biotech). Site-directed mutagenesis of the apoA-I WT cDNA (R173C, R173P, L170P, and P143R) was performed by PCR using Quick Change II XL Site-Directed Mutagenesis Kit and pairs of oligonucleotides carrying the desired mutations (Table 1). The clones were verified by endonuclease digestion and sequencing (GATC Biotech).

The target proteins were expressed as His-tagged fusion proteins in *E. coli* BL21 (DE3) cells (Invitrogen). The presence of the small His-tag in recombinant apoA-I proteins has previously been reported not to interfere with the analyses. In conformational analyses reported in a previous study, no significant differences were observed between His-tag containing wild-type apoA-I and apoA-I after the removal of the His-tag or commercial apoA-I [16]. The cells containing the expression constructs were cultured in Luria-Bertani medium supplemented with 50 mM kanamycin sulphate at 37 °C until the cell density reached an OD_{600} of 0.6–0.7. The expression of proteins was induced with isopropyl-β-D-thiogalactopyranoside (IPTG) (1 mM final concentration) by incubating the culture for 5–6 h in the case of WT, P143R, and R173C proteins and for 2.5–3 h in the case of L170P and R173P proteins. Thereafter, the cells were harvested by centrifugation at 6000×*g* for 10 min at 4 °C. The bacterial pellet was resuspended in lysis buffer and lysed by repeated freeze–thaw cycle followed by sonication. The lysate was centrifuged at 13,000×*g* for 10 min at 4 °C and the supernatant was passed through the Ni-NTA column (Novagen). The column was subsequently washed (with resuspension buffer and 10 mM imidazole) and the fusion proteins were eluted using 100 mM imidazole containing elution buffer (0.5 M Tris, 1% EDTA). The purity of proteins was confirmed by SDS-polyacrylamide gel electrophoresis and the concentration was determined using BCA assay. The purified proteins were also confirmed by western blot analysis using anti-His-tag antibody (data not shown). The purified proteins were dialyzed extensively against 50 mM Tris buffer and concentrated using Amicon centrifugal filter (with a molecular weight cut-off of 10 kDa). The purified protein stock solutions were stored in the dark at 4 °C and were used within 4 weeks. For long term storage, the proteins were aliquoted and flash-frozen in liquid nitrogen prior to storage at −80 °C.

2.3. Intrinsic fluorescence analysis and ANS binding assay

ApoA-I WT and its variants were diluted from the stock solutions in 50 mM Tris-HCl buffer (pH 7.4). Intrinsic fluorescence emission spectra corresponding to the average signal from naturally occurring Trp (8, 50, 72, and 108) and Tyr (18, 29, 100, 115, 116) residues in the primary sequence of the proteins were recorded over the 300–500 nm range at 25 °C with an Agilent Cary Eclipse fluorescence spectrophotometer using a 10-mm cell, following excitation at 295 (Trp) and 280 nm (Trp/Tyr). Emission spectra were acquired at a scan speed of 300 nm/min, with 10 and 5 slit widths for excitation and emission, respectively.

Conformational changes in the tertiary structure of protein with consequent changes in the hydrophobicity of the protein surface of apoA-I WT and its variants were analyzed by ANS binding assay. Emission fluorescence spectra of the proteins diluted in 50 mM Tris

Table 1
List of primers used for preparing mutant apoA-I.

Proteins	Primer (5′–3′)
P143R	**Forward:** GCAAGAGAAGCTGAGCAGACTGGGCGAGGAGATG
	Reverse: CATCTCCTCGCCCAGTCTGCTCAGCTTCTCTTGC
V156E	**Forward:** GCGCGCCCATGAGGACGCGCTGC
	Reverse: GCAGCGCGTCCTCATGGGCGCGC
L170P	**Forward:** CAGCGACGAGCCGCGCCAGCGCT
	Reverse: AGCGCTGGCGCGGCTCGTCGCTG
R173C	**Forward:** AGCTGCGCCAGTGCTTGGCCGCG
	Reverse: CGCGGCCAAGCACTGGCGCAGCT
R173P	**Forward:** GCTGCGCCAGCCCTTGGCCGCGC
	Reverse: GCGCGGCCAAGGGCTGGCGCAGC

buffer (pH 7.4) at 25 °C were examined in the presence of ANS dye. The concentrations of proteins and ANS used were 100 μg/mL and 250 μM, respectively. Emission spectra were recorded over a scan range of 400–700 nm, with excitation at 380 nm, in three independent experiments. A scan speed of 300 nm/min, with 10 and 5 slit width, was used for excitation and emission, respectively.

2.4. Circular dichroism spectroscopy

The secondary and tertiary structures of proteins were analyzed by far- (185–260 nm) and near-UV (260–360 nm) CD measurements, respectively, carried out using a JascoJ-1500 CD spectrometer set at 25 °C after extensive purging with N_2 at a scan speed of 20 nm/min. The proteins (0.1 mg/mL for far-UV CD and 1 mg/mL for near-UV CD) in 10 mM Tris-HCl buffer (pH 7.4) were subjected to CD measurements using 0.1 cm and 1 cm quartz cuvettes. The averages of three scans were baseline-subtracted [17–19].

2.5. FTIR spectroscopy

For exploring the structural transitions associated with the aggregation process, FTIR analysis was done. Spectra were recorded on a 100 FTIR spectrometer (PerkinElmer Inc., USA). Aliquots (40 μL) of 0.5 mg/mL apoA-I in 10 mM Tris-HCl (pH 7.4) were withdrawn after incubation at 4 and 37 °C (at day 4) and were spread uniformly on the surface of a germanium crystal using N_2 to form a hydrated thin film. Spectra were scanned over the range of 400–4000 cm^{-1} at a resolution of 2 cm^{-1} under continuous N_2 purging [20]. The spectra presented herein are the averages of the three determinations.

2.6. Thioflavin T and Congo red binding assay

Identification of amyloid fibrils was done by monitoring the changes in the absorbance of the azo dyes, ThT and congo red, to assess the aggregability/amyloidogenicity of the purified proteins. ThT stock solution was prepared by dissolving 8 mg of ThT in 10 mL of 50 mM Tris-HCl buffer, pH 7.0, and was filtered through a 0.2 μm syringe filter. One milliliter of this solution was added to 50 mL of Tris-HCl buffer on the day of analysis to generate the working solution. An aliquot (5–10 μL) of protein incubated overnight at 37 °C with agitation on a shaker incubator was added to 1 mL of working solution and stirred for 1 min. The fluorescence intensity was recorded in the scan range of 450–550 nm using an Agilent Cary Eclipse fluorescence spectrophotometer after excitation at 440 nm (slit width 5 nm) [21,22]. The congo red stock solution (7 mg/mL) prepared in 50 mM Tris-HCl buffer was filtered through a 0.2 μm syringe filter. A 5 μL aliquot of this solution was added to 1 mL of 50 mM Tris-HCl buffer, which was used as a control. Furthermore, 5–10 μL of protein sample was added to the solution and scanned between 400 and 700 nm using a UV–Vis spectrophotometer (Eppendorf) at room temperature in a disposable cuvette. Upon binding to amyloid fibrils, the intensity was increased with a maximum intensity wavelength shift toward 512 nm. The spectra were the average of three determinations [23].

2.7. Thermal and chemical denaturation assay

Thermal unfolding data is used to determine the T_m of a macromolecule, which provides a measure of its thermal stability. Temperature-dependent denaturation of proteins (0.01 mg/mL) was analyzed as a function of increasing temperature (20–85 °C) using a Jasco V-550 UV–Vis double beam spectrophotometer with Peltier temperature controller.

Chemical denaturation of proteins was carried out to study the stability of proteins in the presence of a denaturing agent, guanidine hydrochloride (GndHCl). Proteins (0.3 mg/mL) were incubated at 4 °C overnight prior to the addition of the denaturant, diluted from a 6 M stock solution. The samples were again stored at 4 °C overnight before data collection. Changes in the tryptophan fluorescence intensity were recorded. Unfolding transition of proteins was monitored by recording the wavelength (λ_{max}) of the maximum fluorescence intensity. The reading obtained was the average of two independent dilutions of each sample plotted against the denaturant concentration and $D_{1/2}$ was calculated.

Sigmoidal curves were fitted by the non-linear regression fit of the data according to Boltzmann equation using GraphPad Prism version 8.0. Assuming a two-state model, free energy of denaturation was calculated using the equation, $\Delta G_D = -RTlnK_D$. Each experiment was performed in duplicate.

2.8. Limited proteolysis

Limited proteolysis of 5 mg protein in 10 mM Tris-HCl buffer, pH 7.4, was performed at 1:2000 ratio (w/w) of protein and high purity trypsin (#C3142, Sigma-Aldrich) for the indicated period of time at 25 °C in a shaking water bath [24]. The reaction was stopped with protease inhibitor cocktail followed by addition of SDS gel loading buffer. The proteolytic products were separated by SDS PAGE.

2.9. DMPC clearance assay

Interactions of the proteins with DMPC were monitored by the method of Zhu et al. (2005) [14], with slight modifications. Multilamellar liposomes (MLV) were prepared from a stock solution of DMPC in chloroform. DMPC was dried under an atmosphere of N_2 and resuspended in 50 mM Tris-HCl buffer at pH 7.4, by vortexing for 3–5 min at 24 °C. The proteins (0.3 mg/mL) were incubated at 24 °C with DMPC MLV at a 3:1 (w/w) molar ratio (lipid:protein). The absorbance was monitored at 325 nm for 90 min using a Thermo Scientific Varioskan Flash multi plate reader at a temperature 24 °C.

2.10. Statistical analysis

The spectra are the average of three or two independent experimentations and are represented as means ± SD. Differences between groups were examined for significance using one way ANOVA and Tukey's multiple comparisons test using Graphpad Prism 8.0. The values of $^{*}P < 0.05$, $^{**}P < 0.01$, $^{***}P < 0.001$, and $^{****}P < 0.0001$ were considered statistically significant whereas $^{\#}P > 0.05$ signifies non-significant results.

3. Results and discussion

3.1. Changes in the intrinsic structural conformation and hydrophobicity of apoA-I variants

The intrinsic fluorescence intensity and shift in the emission wavelength maxima were evaluated to compare the tertiary structure of the apoA-I variants. The four naturally occurring tryptophan (at positions 8, 50, 72, and 108 from the N-terminus) and five tyrosine (at positions 18, 29, 100, 115, and 116 from the N-terminus) residues are preserved in all the five selected variants. Fluorescence spectra were obtained either by excitation at 295 nm [25], at which the contribution of tyrosine residues is negligible (Fig. 1a), or by excitation at 280 nm, in which case both tryptophan and tyrosine residues contribute to the absorption (Fig. 1b). The fluorescence intensity maxima for P143R and R173C were similar to that recorded for WT (λ_{max} = ~335 nm), whereas L170P (λ_{max} = ~347 nm), V156E (λ_{max} = ~341 nm), and R173P (λ_{max} = ~341) had the maximum fluorescence intensity at longer wavelengths, consistent with the results of Rosú et al. [26].

The V156E, L170P, and R173P variants showed conformational changes in the tertiary structure, with consequent exposure of the hydrophobic protein surface. Glutamic acid is known to be involved in the

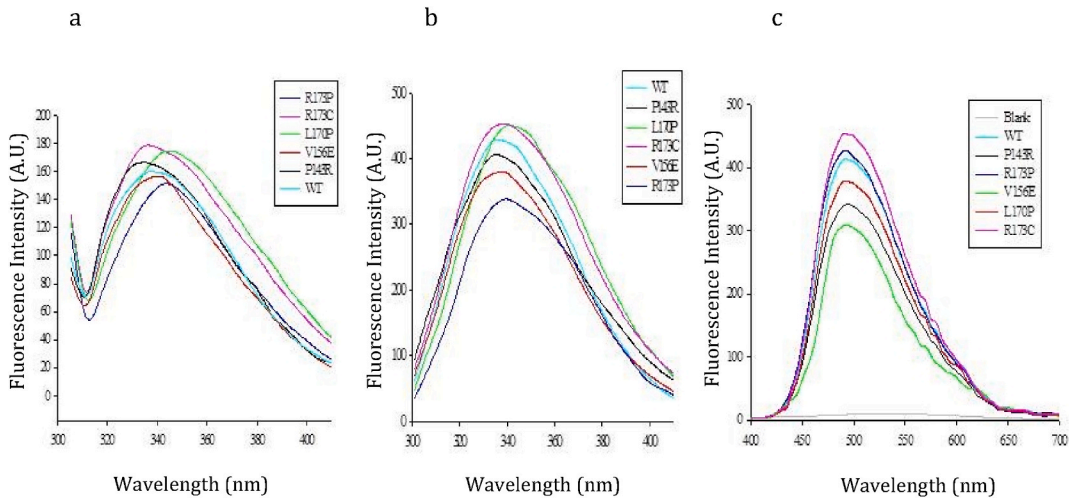

Fig. 1. Intrinsic fluorescence analysis. Tryptophan and tyrosine emission spectra of WT, R173C, L170P, R173P, P143R, and V156E apoA-I at pH 7.4. Excitation was done at 295 nm for tryptophan (a) and at 280 nm for tyrosine/tryptophan (b). Binding of ANS (250 μM) to 100 μg/mL of apoA-I proteins (WT, R173C, L170P, R173P, P143R, and V156E). Excitation was done at 380 nm (c). The spectra were obtained for three independent experiments.

formation of salt bridges, stabilizing the protein tertiary structure. Proline substitution disrupts the α-helical structure and destabilizes the structure of protein. A similar pattern was obtained when the contribution of both tyrosine and tryptophan was analyzed (Fig. 1b). This might lead to increased exposure of hydrophobic residues, as demonstrated by the increase in intrinsic fluorescence intensity.

To get further insights into the tertiary structure of the proteins, ANS binding assay was performed. Several-fold increase in ANS fluorescence intensity in the presence of apoA-I WT was observed. An increase in fluorescence quantum yield was noted for R173C and R173P relative to that for WT. However, V156E, L170P, and P143R exhibited lower quantum fluorescence intensity than WT (Fig. 1c), indicating that the hydrophobic moieties of R173C and R173P are more exposed to the solvent compared to those of the other mutants.

3.2. Structure perturbations due to substitution mutation

Far-UV CD analysis was used to determine the secondary structure of the purified apoA-I WT and its variants in 50 mM Tris-HCl buffer (pH 7.4) at a concentration of 0.1 mg/mL under physiological conditions. The secondary structures were determined using the K2D2 software (Fig. 2a) [27]. The α-helical content for WT and R173C was almost similar, but was higher in the case of P143R and V156E. On the contrary, lower helical structure was observed for L170P and R173P, with an increase in the β-sheet content (Table 2), indicating an altered protein conformation toward aggregate-competent state.

Table 2
Content of α-helix and β-strand (%) in apoA-I WT and its variants as determined using the K2D2 software. Data shown are the means from two independent experiments.

	WT	P143R	V156E	L170P	R173C	R173P
α-helix (%)	61.33 ± 0.004	67.45 ± 0.01	62.00 ± 0.002	47.79 ± 0.01	60.86 ± 0.03	52 ± 0.04
β-sheet (%)	4.06 ± 0.01	3.24 ± 0.03	3.51 ± 0.002	10.33 ± 0.005	4.33 ± 0.02	8.29 ± 0.002

Tertiary structures of the WT and mutant proteins were characterized using near-UV CD **(Fig. 2b)**. A molten globular-like state for apoA-I has been suggested. Several experimentally observed properties of lipid-free apoA-I under near physiological plasma conditions are consistent with the molten globular state: these include well-defined secondary structure folded in a compact globule [28], low unfolding cooperativity, loose tertiary contacts, exposed hydrophobic regions, tendency to aggregate, and high susceptibility to denaturants [29–31]. The spectra of apoA-I WT and its variants were found to be significantly similar, although L170P and R173P showed slightly lower intensity from 260 to 290 nm.

The wavelength shifts at 292 nm in the case of V156E, P143R, and L170P were also observed. The change in the pattern indicates substantial structural arrangement among the aromatic amino acid residues. The decrease in ellipticity suggests that an increasing number of

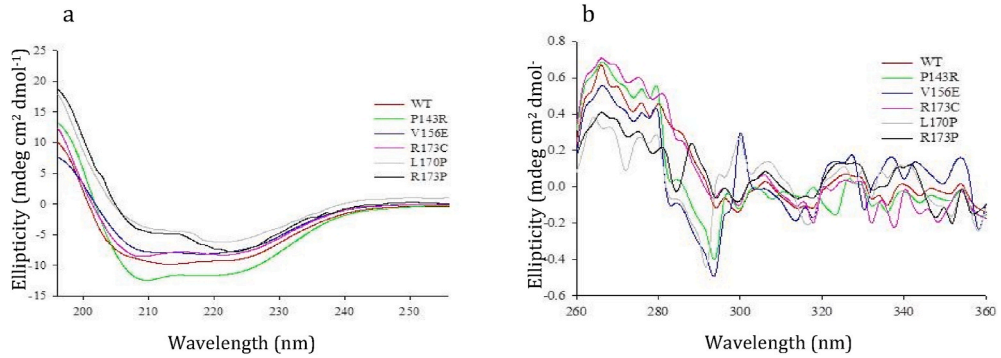

Fig. 2. Far- and near-UV CD spectral analysis. (a) Spectra acquired at 25 °C with 0.1 mg/mL protein concentration in 50 mM Tris-HCl buffer, pH 7.4. (b) Spectra acquired at 25 °C with 1 mg/mL protein concentration in 50 mM Tris-HCl buffer, pH 7.4. Experiments were repeated two times, and data are expressed as means ± SD.

aromatic side-chains are exposed, and these changes are most probably related to the loss of native structure. It is to be expected that a balance between protein compactness, partial unfolding, exposed moiety as well as flexibility might also be responsible for protein amyloidogenecity.

3.3. Detection of cross beta/amyloid structure

The structural transitions associated with the aggregation of proteins were investigated by FTIR analysis on day 1 and day 4 after incubation at 37 °C (Fig. 3a–f). Previous studies have reported a peak for apoA-I near 1650 cm^{-1}, which is characteristic of α-helical proteins. After being converted into fibrils, the peak shifts toward ~1630 cm^{-1}, indicating the high content of β-structure in the fibrils [32–34].

Changes in the wavelength at amide I region in the constituent secondary structural elements of proteins before and after incubation at 37 °C for fibrillation are shown. The results show an insignificant shift in the peaks for apoA-I WT and V156E, indicative of few or no fibrils with β strand conformation, in agreement with the results reported previously for apoA-I WT [35]. P143R and R173C did not show any shift even after day 4 of incubation at 37 °C.

However, L170P and R173P showed a significant shift in the peak toward ~1630, (***P < 0.0001) with a concomitant increase in percentage transmittance. The shifts in the peaks at day 1 and day 4 are shown in Fig. 3g. This depicts the conversion of soluble α-helical forms of these mutants into β-structure enriched fibrils after day 4 of incubation at 37 °C, suggesting the presence of amyloid plaques. A major change in the percentage transmittance was also observed, which might be due to the aggregation propensity of these mutants. We also observed a several fold percentage increase in transmittance of secondary structure elements in apoA-I WT and its mutants as a function of time of incubation, as indicated by the shift in maximum intensity in FTIR analysis.

3.4. Examination of stability of the apoA-I variants as a function of temperature and GdnHCl denaturation

Thermal unfolding of free apolipoproteins is thermodynamically reversible below the melting temperature but becomes irreversible beyond this temperature [31]. This pattern was also observed in the present study wherein we studied thermal denaturation over a temperature range of 20–85 °C. A sigmoidal curve gives an idea that the proteins were structurally stable up to ~50 °C. The thermal stability of the WT and mutated forms of apoA-I was further determined by observing the unfolding of the proteins (Fig. 4a).

The values of the melting temperature (T_m), Gibbs free energy (ΔG^{o}_{D}), melting enthalpy of thermal unfolding (ΔH_m), and change in the heat capacity (ΔCp) calculated from the data obtained by UV–Visible spectrophotometry are presented in Table 3. Compared to the denaturation

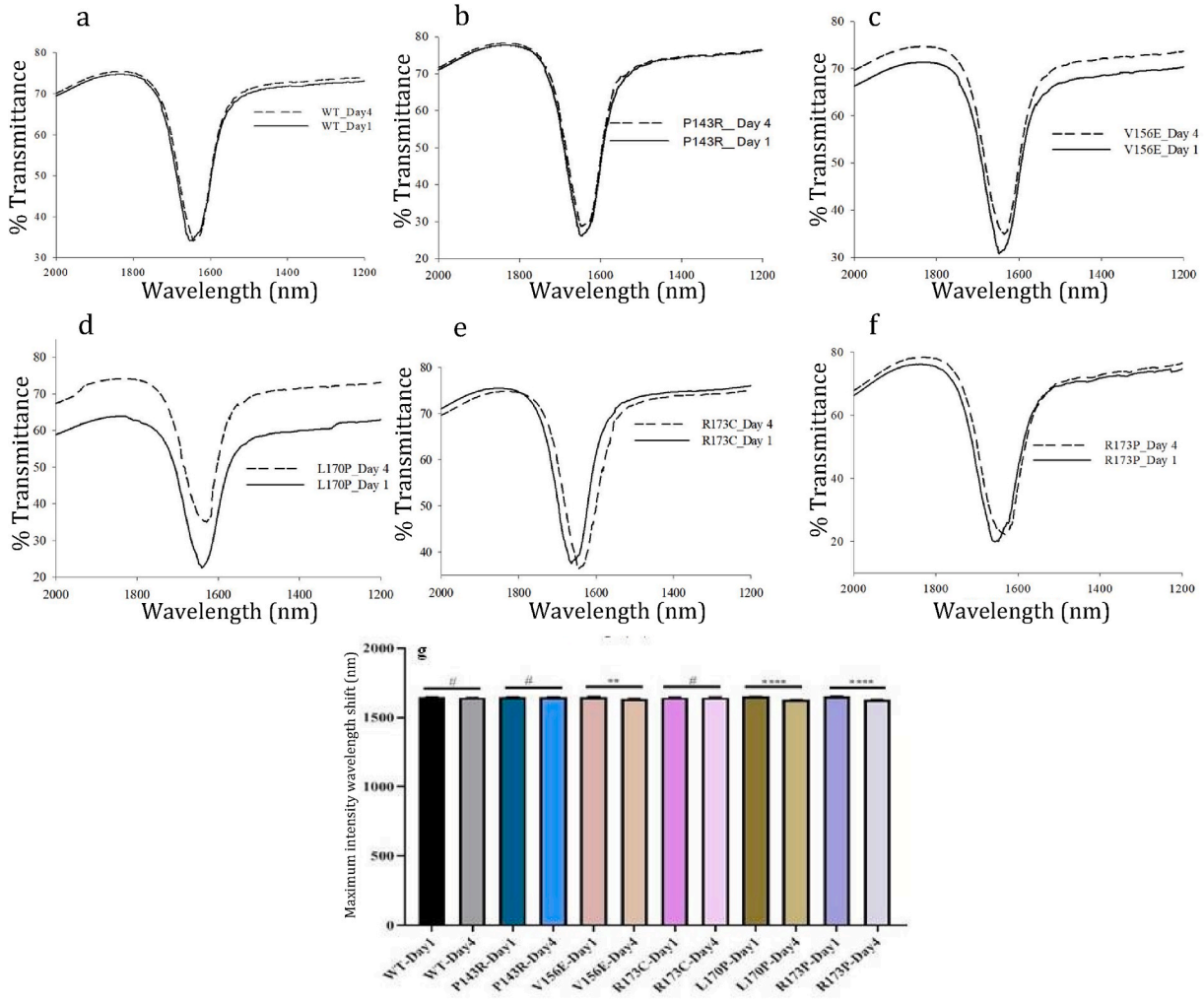

Fig. 3. FTIR spectroscopy. The spectra obtained on day 1 and day 4 after incubation at 37 °C at pH 7.4 in 50 mM Tris-HCl buffer. The spectra are averages of three independent experiments (a)–(f). Shift in the wavelength peak after incubation at 37 °C for 4 days. Each value is the mean ± SD of three experiments. *P < 0.05, **P < 0.01, ***P < 0.001, and ****P < 0.0001 with respect to the values on day 1. #P > 0.05 signifies non-significant differences (g).

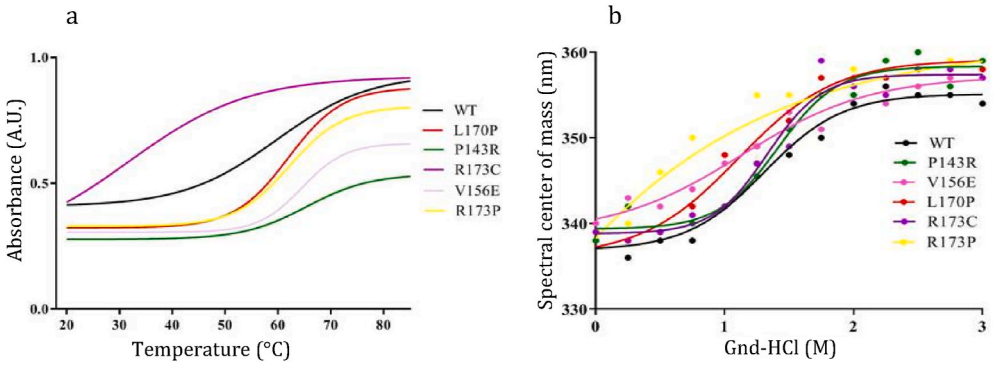

Fig. 4. Temperature and chemical dependent folding and unfolding. Absorbance spectra at 280 nm were recorded over a range of temperature from 20 to 85 °C (a). Proteins (0.1 mg/mL) were incubated in 10 mm Tris-HCl buffer at pH 7.4 with increasing concentrations of GndHCl. Trp fluorescence emission spectra were obtained by excitation at 295 nm (b). The spectra are averages of three independent experiments.

Table 3
Thermodynamic parameters of the different apoA-I variants under denaturing conditions.

Proteins	Temperature denaturation				GndHCl denaturation	
	T_m (°C)	ΔH_m (kcal mol^{-1})	ΔC_p (kcal mol^{-1} K^{-1})	ΔG°_D (kcal mol^{-1})	$D_{1/2}$ (M)	ΔG°_D (kcal mol^{-1})
WT	55.3 ± 0.3	37 ± 2.3	1.52 ± 0.15	1.7 ± 0.15	1.3 ± 0.1	1.6 ± 0.4
P143R	47.1 ± 0.4	31 ± 2.3	1.25 ± 0.12	1.2 ± 0.13	1.4 ± 0.1	1.6 ± 0.2
V156E	62.6 ± 0.3	58 ± 1.9	1.51 ± 0.14	3.9 ± 0.14	1.1 ± 0.2	0.8 ± 0.3
R173C	45.9 ± .03	28 ± 1.4	1.13 ± 0.08	1.2 ± 1.2	1.3 ± 0.1	1.8 ± 0.4
R173P	53.3 ± 0.1	42 ± 1.7	1.29 ± 0.12	2.1 ± 0.15	1.1 ± 0.1	0.13 ± 0.1
L170P	55.6 ± 0.2	39 ± 1.5	1.21 ± 0.15	1.9 ± 0.12	1.1 ± 0.1	1.2 ± 0.3

curve of the two-state model of WT, R173C displayed a decreased cooperative behavior of unfolding as indicated by the shallowness in the curve and, therefore, the mutation destabilized the protein. P143R, R173P, V156E, and L170P had greater stability in comparison to WT and R173C.

The folding of apoA-I and its variants in the presence of GdnHCl was monitored to investigate the stability of the proteins against chemical denaturation. As per the two-state model system, the sigmoid curve confirmed the cooperative nature of the unfolding of the proteins (Fig. 4b). R173P and V156E showed a decrease in the cooperative nature of proteins. Hyperbolic curve is an indication of faster and non-cooperative unfolding behavior. The calculated midpoint of the denaturation ($D_{1/2}$) and Gibbs free energy (ΔG^{o}_{D}) are tabulated in Table 3.

In contrast to the WT, P143R, and R173C, the R173P and V156E mutants had altered structural properties as indicated by their decreased interaction with guanidine hydrochloride (higher midpoint of denaturation), a marginally higher stability, and a small red shift in tryptophan maximum wavelength fluorescence intensity. The P143R mutant appeared to have a slightly higher stability. Interestingly, we observed that the stability of V156E was more upon thermal denaturation whereas it was less upon GdnHCl-induced unfolding. Although based on our results we cannot definitively comment on it, we can surmise that this could be due to the presence of an ionic interaction in the V156E protein that is not disturbed at higher temperatures but is susceptible to GdnHCl. Because in this mutant a non-polar hydrophobic residue (Val) in the middle of the non-polar face of helix-6 of the protein structure is being replaced with a charged (Glu) residue, which may lead to structural alterations in apoA-I in its hinge region, we believe that the introduced charged residue is involved in some ionic interaction that is resistant to breaking by heating but is susceptible to breakage by GdnHCl, an ionic detergent. Moreover, there is a possibility that such extra ionic interaction resulting from the introduction of Glu might get masked in the presence of GdnHCl. Such masking of ionic interactions in proteins because of the ionic nature of GdnHCl has previously been reported [36]. Another possibility could be that the introduction of an extra Glu residue increases the T_m of the protein, as has been reported previously for *E*TRX protein, wherein the replacement of an Asp with Glu increased the T_m by 1.5 °C [37]. Thus, there could be any of the above or other reasons that might be responsible for the higher stability upon thermal denaturation compared with that observed for chemical denaturation induced by GdnHCl.

3.5. Assessment of amyloid fibril formation by ThT and Congo red

Thioflavin T (ThT) assay is used to monitor the amyloidogenic propensity of proteins [38]. We observed that WT and the mutants differed in their ability to bind the amyloidophilic ThT dye. ApoA1WT ($^{\#}P > 0.05$), R173C ($^{\#}P > 0.05$), P143R ($^{\#}P > 0.05$) did not show much affinity toward ThT, indicating negligible transition to β sheet after incubation, whereas V156E ($^{**}P < 0.01$) did show some affinity. L170P and R173P had significant affinity toward the dye in comparison to WT ($^{****}P < 0.0001$). Binding of ThT, followed by an increase in the fluorescence (Fig. 5a), suggests the formation of amyloid-like molecular structure.

Whether *in vitro* incubation of apoA-I under amyloidogenic conditions resulted in the formation of apoA-I fibrils or aggregates was also checked by congo red assay. After addition of congo red, a significant increase in the absorbance was observed for all the mutant forms of apoA-I as well as for WT (Fig. 5b), indicating the presence of aggregates. Along with increased intensity, a red shift of the absorption maximum (from ~490 nm toward ~512 nm) was noted after binding with amyloid, specifically in the case of R173P, indicating the presence of fibrils. However, the other variants did not show any major wavelength shift.

3.6. Proteolytic susceptibility

After incubation with trypsin for the indicated time periods, WT, R173C, and V156E showed a similar profile and remained stable even after 240 min of incubation, indicating almost identical folding. However, P143R and R173P showed increased and rapid protease sensitivity, indicating a loose tertiary structure. L170P also showed increased protease sensitivity (Fig. 6a–f).

Our results also revealed that R173C did not show intrinsic propensity for the crossed β-sheet fibrils and/or amorphous aggregates. The lower proteolytic susceptibility of R173C is unexpected because the mutation is located in the hot spot domain of apoA-I where the substitution of amino acid is reported to be associated with increased fibril

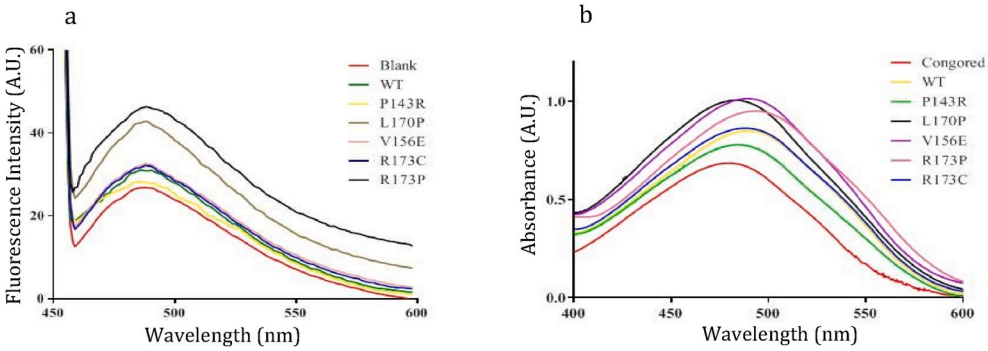

Fig. 5. Evaluation of amyloidogenic propensities of apoA-I variants. (a) Aggregate/amyloid determination of WT and its mutants. ApoA1 WT, R173C, L170P, P143R, V156E, and R173P were incubated with ThT solution at 37 °C and fluorescence was measured at an excitation wavelength of 440 nm. (b) Proteins under analysis were incubated overnight at 37 °C in 50 mM Tris-HCl buffer. Binding of congo red dye to protein induces a characteristic increase in absorbance as well as red shift from 490 toward 512 nm. The spectra are averages of three independent experiments. Each value is the mean ± SD for three experiments. (For interpretation of the references to color in this figure legend, the reader is referred to the Web version of this article.)

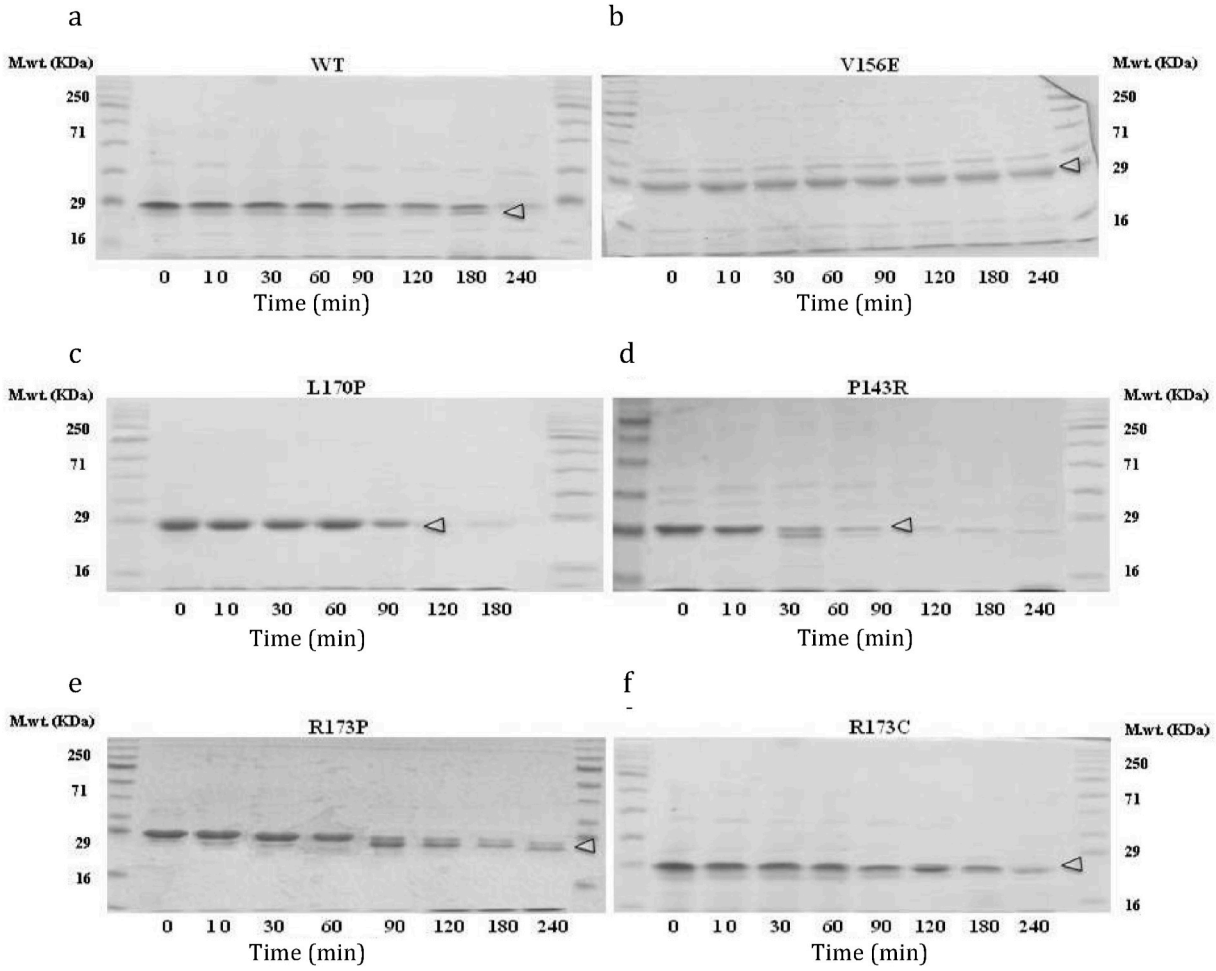

Fig. 6. Limited proteolysis analysis of apoA-I variants. Proteins (5 μg) were incubated for the mentioned periods of time at 25 °C in the presence of trypsin. The cleaved peptides were separated by SDS-PAGE and visualized after staining with Coomassie dye.

formation. This might be due to its ability for covalent disulfide bridge formation that maintains protein stability [13].

3.7. Clearance of DMPC liposomes

One of the most important biological activities of apoA-I is to interact with lipids and form lipoproteins, which is of major interest in lipoprotein metabolism and function. It was observed that all the selected variants readily solubilized the DMPC liposomes (Fig. 7), but surprisingly, the V156E and L170P mutants showed more rapid kinetics than the WT and other mutants. The half-life ($t_{1/2}$) for liposome clearance was 13 ± 2 min for WT, 4 ± 1 min for L170P, 15 ± 0.2 min for R173P, 6.5 ± 0.5 min for V156E, and 23.5 ± 0.5 min for R173P and P143R, which shows that L170P and V156E are associated with greater clearance rates.

This may be because V156E is mostly monomeric at the concentration used, whereas the other protein solutions may also contain some oligomeric forms [15]. Alternatively, the introduction of a glutamate in

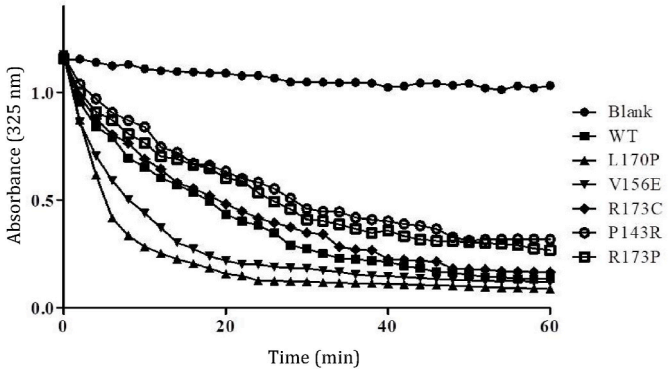

Fig. 7. Kinetics of interaction of the selected apoA-I variants with DMPC multilamellar liposomes. The reaction was initiated by addition of 0.3 mg/mL of protein to the multilamellar DMPC liposomes at pH 7.4. DMPC to protein ratio was 3:1 (w/w). Absorbance at 325 nm was monitored at an interval of 2 min for up to 1 h at 24 °C. The spectra are averages of three independent experiments. Values are means ± SD for three experiments.

the sequence may lead to salt bridge formation with an adjacent basic residue, thus, significantly decreasing the polarity and hydration property. This would promote interaction with the DMPC bilayer. In the case of P143R mutant, the decreased rate of DMPC lysis may be attributed either to the decrease in α-helical structure or to excess charge in this mutant. Substitution of an arginine by a proline in the 'hotspot' domain of ApoA1 may result in a drastic change in protein functionality and metabolism [7].

4. Conclusion

We conclude that structural characteristics determining the amyloidogenecity are not common for all the mutants. A correlation was established between the propensity of R173P and L170P to misfold and their stability; under physiological conditions, the natural variants showed significantly lower cooperativity compared to the WT form, together with the partial loss of secondary structure, which contributes to the higher aggregation tendency. Nevertheless, the mutants depict a significant difference, which indicates a cause-and-affect relationship in ApoA1 associated amyloidoses. We observed that (i) In general, R173C and V156E display approximately similar α-helical structure with respect to the native WT, whereas increase in β-sheet is observed in the case of L170P and R173P; (ii) more exposed hydrophobic moiety, particularly in the case of L170P; (iii) increased aggregation propensity in the case of L170P and R173P; (iv) higher proteolytic susceptibility of P143R and L170P.

Conflicts of interest

The authors declare no potential conflicts of interest.

Funding

This research did not receive any specific grant from funding agencies in the public, commercial, or not-for-profit sectors.

CRediT authorship contribution statement

Farah Ma'arfi: Methodology, Validation, Formal analysis, Investigation, Data curation, Visualization, Writing - original draft, Writing - review & editing. **Subhash Chandra:** Methodology, Validation, Investigation, Data curation, Visualization. **Jamal e Fatima:** Methodology, Formal analysis, Investigation, Data curation. **Mohd Yasir Khan:** Methodology, Formal analysis, Investigation, Data curation. **Snober S. Mir:** Formal analysis, Methodology, Resources, Data curation. **Mohd Aslam Yusuf:** Conceptualization, Methodology, Validation, Formal analysis, Investigation, Visualization, Resources, Writing - original draft, Writing - review & editing, Supervision, Project administration.

Declaration of competing interest

The authors declare that they have no known competing financial interests or personal relationships that could have appeared to influence the work reported in this paper.

Acknowledgments

The authors are thankful to Prof. Neera Bhalla Sarin, School of Life Sciences, Jawaharlal Nehru University, New Delhi for her invaluable infrastructural support to carry out some of the experiments and to Dr. Uzma Fatima, Recdesprot Pvt. Ltd., Chandigarh for valuable suggestions. The manuscript communication number assigned by the Dean, R&D, Integral University, Lucknow is IU/R&D/2019-MCN000649.

References

[1] L. Pastore, L.M. Belalcazar, K. Oka, R. Cela, B. Lee, L. Chan, A.L. Beaudet, Helper-dependent adenoviral vector-mediated long-term expression of human apolipoprotein AI reduces atherosclerosis in ApoE-deficient mice, Gene 327 (2004) 153–160.
[2] C.G. Brouillette, G.M. Anantharamaiah, J.A. Engler, D.W. Borhani, Structural models of human apolipoprotein AI: a critical analysis and review, Biochim. Biophys. Acta 1531 (2001) 4–46.
[3] R. Gaglione, G. Smaldone, R. Di Girolamo, R. Piccoli, E. Pedone, A. Arciello, Cell milieu significantly affects the fate of ApoAI amyloidogenic variants: predestination or serendipity? Biochim. Biophys. Acta 1862 (2018) 377–384.
[4] A.R. Tall, Cholesterol efflux pathways and other potential mechanisms involved in the atheroprotective effect of high-density lipoproteins, J. Intern. Med. 263 (2008) 256–273.
[5] D.J. Rader, E.T. Alexander, G.L. Weibel, J. Billheimer, G.H. Rothblat, The role of reverse cholesterol transport in animals and humans and relationship to atherosclerosis, J. Lipid Res. 50 (Supplement) (2009) S189–S194.
[6] G.H. Rothblat, F.H. Mahlberg, W.J. Johnson, M.C. Phillips, Apolipoproteins, membrane cholesterol domains, and the regulation of cholesterol efflux, J. Lipid Res. 33 (1992) 1091–1097.
[7] M.G. Sorci-Thomas, M.J. Thomas, The effects of altered apolipoprotein AI structure on plasma HDL concentration, Trends Cardiovasc. Med. 12 (2002) 121–128.
[8] C.R. Sirtori, L. Calabresi, G. Franceschini, D. Baldassarre, M. Amato, J. Johansson, M. Salvetti, C. Monteduro, R. Zuli, M.L. Muiesan, E. Agabiti-Rosei, Cardiovascular status of carriers of the apolipoprotein A-IMilano mutant: the Limone Sul Garda study, Circulation 103 (2001) 1949–1954.
[9] L. Obici, G. Franceschini, L. Calabresi, S. Giorgetti, M. Stoppini, G. Merlini, V. Bellotti, Structure, function and amyloidogenic propensity of apolipoprotein AI, Amyloid 13 (2006) 191–205.
[10] G.I. Mucchiano, B. Häggqvist, K. Sletten, P. Westermark, Apolipoprotein A1-derived amyloid in atherosclerotic plaques of the human aorta, J. Pathol. 193 (2001) 270–275.
[11] S. Raimondi, F. Guglielmi, S. Giorgetti, S. Di Gaetano, A. Arciello, D.M. Monti, et al., Effects of the known pathogenic mutations on the aggregation pathway of the amyloidogenic peptide of apolipoprotein AI, J. Mol. Biol. 407 (2001) 465–476.
[12] G.M. Gaddi, R.A. Gisonno, S.A. Rosú, L.M. Curto, E.E. Elías, E.D. Prieto, et al., N-terminal mutants of human apolipoprotein AI: structural perturbations associated to protein misfolding, BioRxiv (2019) 520171.
[13] J. Petrlova, J. Dalla-Riva, M. Mörgelin, M. Lindahl, E. Krupinska, K.G. Stenkula, et al., Secondary structure changes in ApoA-I Milano (R173C) are not accompanied by a decrease in protein stability or solubility, PLoS One 9 (2014), e96150.
[14] X. Zhu, G. Wu, W. Zeng, H. Xue, B. Chen, Cysteine mutants of human apolipoprotein AI: a study of secondary structural and functional properties, J. Lipid Res. 46 (2005) 1303–1311.
[15] K.H. Cho, D.M. Durbin, A. Jonas, Role of individual amino acids of apolipoprotein AI in the activation of lecithin: cholesterol acyltransferase and in HDL rearrangements, J. Lipid Res. 42 (2001) 379–389.
[16] R. Del Giudice, A. Arciello, F. Itri, A. Merlino, M. Monti, M. Buonanno, et al., Protein conformational perturbations in hereditary amyloidosis: differential impact of single point mutations in ApoAI amyloidogenic variants, Biochim. Biophys. Acta 1860 (2016) 434–444.
[17] N.J. Greenfield, Using circular dichroism spectra to estimate protein secondary structure, Nat. Protoc. 1 (2006) 2876–2890.
[18] J. Petrlova, T. Duong, M.C. Cochran, A. Axelsson, M. Mörgelin, L.M. Roberts, J. O. Lagerstedt, The fibrillogenic L178H variant of apolipoprotein AI forms helical fibrils, J. Lipid Res. 53 (2012) 390–398.
[19] J. Dalla-Riva, K.G. Stenkula, J. Petrlova, J.O. Lagerstedt, Discoidal HDL and apoA-I-derived peptides improve glucose uptake in skeletal muscle, J. Lipid Res. 54 (2013) 1275–1282.

[20] M.Y. Khan, S. Alouffi, S. Ahmad, Immunochemical studies on native and glycated LDL–An approach to uncover the structural perturbations, Int. J. Biol. Macromol. 115 (2018) 287–299.
[21] R. Khurana, C. Coleman, C. Ionescu-Zanetti, S.A. Carter, V. Krishna, R.K. Grover, et al., Mechanism of thioflavin T binding to amyloid fibrils, J. Struct. Biol. 151 (2005) 229–238.
[22] M. Biancalana, S. Koide, Molecular mechanism of Thioflavin-T binding to amyloid fibrils, Biochim. Biophys. Acta 1804 (2010) 1405–1412.
[23] M.T. Elghetany, A. Saleem, K. Barr, The Congo red stain revisited, Ann. Clin. Lab. Sci. 19 (1989) 190–195.
[24] I. Kheterpal, A. Williams, C. Murphy, B. Bledsoe, R. Wetzel, Structural features of the Aβ amyloid fibril elucidated by limited proteolysis, Biochemistry 40 (2001) 11757–11767.
[25] N.A. Ramella, O.J. Rimoldi, E.D. Prieto, G.R. Schinella, S.A. Sanchez, M. S. Jaureguiberry, et al., Human apolipoprotein AI-derived amyloid: its association with atherosclerosis, PLoS One 6 (2011), e22532.
[26] S.A. Rosú, O.J. Rimoldi, E.D. Prieto, L.M. Curto, J.M. Delfino, N.A. Ramella, M. A. Tricerri, Amyloidogenic propensity of a natural variant of human apolipoprotein AI: stability and interaction with ligands, PLoS One 10 (2015), e0124946.
[27] C. Perez-Iratxeta, M.A. Andrade-Navarro, K2D2: estimation of protein secondary structure from circular dichroism spectra, BMC Struct. Biol. 8 (2008) 25.
[28] D.L. Barbeau, A. Jonas, T.L. Teng, A.M. Scanu, Asymmetry of apolipoprotein AI in solution as assessed from ultracentrifugal, viscometric, and fluorescence polarization studies, Biochemistry 18 (1979) 362–369.
[29] J.A. Reynolds, Conformational stability of the polypeptide components of human high density serum lipoprotein, J. Biol. Chem. 251 (1976) 6013–6015.
[30] A.R. Tall, G.G. Shipley, D.M. Small, Conformational and thermodynamic properties of apo A-1 of human plasma high density lipoproteins, J. Biol. Chem. 251 (1976) 3749–3755.
[31] O. Gursky, D. Atkinson, Thermal unfolding of human high-density apolipoprotein A-1: implications for a lipid-free molten globular state, Proc. Natl. Acad. Sci. U.S.A. 93 (1996) 2991–2995.
[32] G. Vecchio, A. Bossi, P. Pasta, G. Carrea, Fourier-transform infrared conformational study of bovine insulin in surfactant solutions, Int. J. Pept. Protein Res. 48 (1996) 113–117.
[33] J. Wei, L. Xie, Y.Z. Lin, C.L. Tsou, The pairing of the separated A and B chains of insulin and its derivatives, FTIR studies, Biochim. Biophys. Acta 1120 (1992) 69–74.
[34] J. Wei, Y.Z. Lin, J.M. Zhou, C.L. Tsou, FTIR studies of secondary structures of bovine insulin and its derivatives, Biochim. Biophys. Acta 1080 (1991) 29–33.
[35] J. Kong, S. Yu, Fourier transform infrared spectroscopic analysis of protein secondary structures, Acta Biochim. Biophys. Sin. 39 (2007) 549–559.
[36] O.D. Monera, C.M. Kay, R.S. Hodges, Protein denaturation with guanidine hydrochloride or urea provides a different estimate of stability depending on the contributions of electrostatic interactions, Proteome Sci. 3 (1994) 1984–1991.
[37] D.Y. Lee, K.A. Kim, Y.G. Yu, K.S. Kim, Substitution of aspartic acid with glutamic acid increases the unfolding transition temperature of a protein, Biochem. Biophys. Res. Commun. 320 (2004) 900–906.
[38] P.S. Vassar, C.F. Culling, Fluorescent stains, with special reference to amyloid and connective tissues, Arch. Pathol. 68 (1959) 487–498.